Taylor & Francis
Taylor & Francis Group

A review of vasculogenesis models

D. AMBROSI†, F. BUSSOLINO‡ and L. PREZIOSI†*

†Department of Mathematics, Politecnico di Torino, Corso Duca degli Abruzzi, 24 10129, Torino, Italy
‡Division of Molecular Angiogenesis, Institute for Cancer Research and Treatment, 10060 Candiolo, Torino, Italy

Mechanical and chemical models of vasculogenesis are critically reviewed with an emphasis on their ability to predict experimentally measured quantities. Final remarks suggest a possibility to merge the capabilities of different models into a unified approach.

1. Introduction

In the embryo, primitive vascular plexus form by the process of vasculogenesis, where mesoderm-derived precursors of endothelial cells assemble by directed cell migration and cohesion [1–3]. This network is characterized by polygons having a precise size dictated by the principal and paradigmatic function of vasculature: the oxygen transport to the tissues. Therefore the intercapillary distance is dictated by the diffusion coefficient of oxygen. This characteristic is maintained in the adult body where the capillary network embedded in the tissues and stemmed by the vascular tree has the same geometric shape of the minimal unit participating in the formation of embryo vascular net, and is optimal for metabolic exchange [4–6]. The ability to form networking capillary tubes is a cell autonomous property of endothelial cells. At the site of vessel formation soluble stimuli released by neighbouring cells modify the genetic programme of endothelial cells [7] allowing them to be responsive to permissive cues coming from extracellular environment [8]. Nice *in vitro* models support this concept. In particular, it is well known that culturing endothelial cells on a scaffold of Matrigel, a natural basal membrane matrix, markedly accelerates their morphological differentiation in geometric tubular networks that are almost identical to vascular beds formed *in vivo* by vasculogenesis [9, 10]. This phenomenon has been called *in vitro* angiogenesis [11]. The issue of how endothelial cells self-organize geometrically into capillary networks is still rather obscure. How can separate individuals cooperate in the formation of coherent structures? Which is the mechanism regulating the dimension of the patterns?

Answering this question is an issue of great interest in understanding tumour growth but also the reconstitution of a proper and functional vascular network is a major issue in tissue engineering and regeneration. The limited success of current technologies may be related to the difficulties to build a vascular tree with correct geometric ratios for nutrient delivery.

In this review, we focus on mathematical models of *in vitro* vasculogenesis. The readers interested in the description of angiogenesis or wound healing, are referred to Bussolino *et al.* [12], Chaplain and Anderson [13], Little *et al.* [14], and Levine and Sleeman [15].

Section 1 is devoted to experimental facts. The following two sections describe in detail two classes of models: the former is based on the concepts of cell persistence and endogenous chemotaxis, the latter is based on the mechanical interactions with the substratum. The "fors" and "againsts" of the two models are critically discussed. A final section presents some research perspectives.

2. Experimental facts

Vasculogenesis can be obtained *in vitro* using different experimental set-ups, substrata (e.g., Matrigel, fibronectin, collagen, fibrin and semisolid methilcellulose), and cell-lines e.g., human umbilical vein endothelial cells (HUVEC); human dermal microvascular endothelial cells (HDMEC); human capillary endothelial cells (HCEC); human marrow microvascular endothelial cells; bovine

---

*Corresponding author. Email: preziosi@calvino.polito.it

aorthic endothelial cells (BAEC); bovine capillary endothelial cells (BCEC); bovine retin endothelial cells (BREC); rat capillary endothelial cells (RCEC); embryonic stem cells (ESC); calf pulmonary aortic endothelial cells (CPAEC); adrenal capillary endothelial cells (ACEC), as reviewed in Vailhé *et al.* [16]. To this list one could add melanoma cells, which seem to form capillary-like structures by themselves, as described for instance in Hendrix *et al.* [17] and Mariotis *et al.* [18].

The term "vasculogenesis *in vitro*" therefore includes such a large variety of experimental protocols that makes it almost impossible to provide a unified illustration of the biological process. Therefore, in the present section, we refer to the experimental set-up of Serini *et al.* [19]. Differences with other works reported in the literature will be pointed out when needed.

In the experiments by Serini *et al.* [19] a Petri dish is coated with an amount of Matrigel, a surface which favours cell motility and has biochemical characteristics similar to living tissues, having a thickness of $44 \pm 8\,\mu m$. Human endothelial cells from large veins or adrenal cortex capillaries (HUVEC) are dispersed in a physiological solution which is poured on the top of the Matrigel and sediment settles by gravity onto the Matrigel surface. Cells then move on the horizontal Matrigel surface giving rise to a process of aggregation and pattern formation.

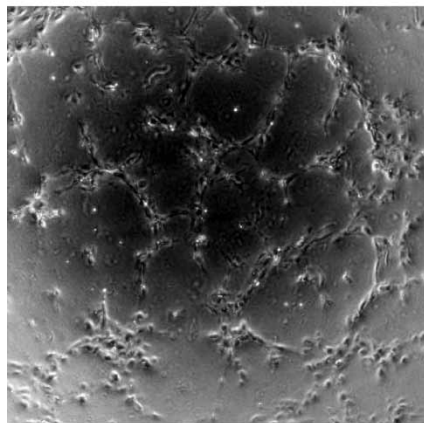The process of formation of a vascular-type network lasts $12-15$ hours and evolves according to the following steps:

(i) In the first 3 to 6 h endothelial cells migrate independently, keeping a round shape until they collide with closest neighbours (figure 1(a,b)) (as observed also by Tranqui and Traqui [20]). It is interesting to note that in this phase cells move much faster than in later phases, and that the motion of the cells seems to be of amoeboid type (see, for instance, Friedl [21] Webb and Horwitz [22] and Wolf *et al.* [23]).

(ii) The cells eventually form a continuous multicellular network (figure 1(c)) and "splat" on the Matrigel multiplying the number of adhesion sites.

(iii) The network slowly moves as a whole, undergoing a slow thinning process (figure 1(d)), probably driven by a stress field generated by mutual traction, which, however, leaves the network structure mainly unaltered.
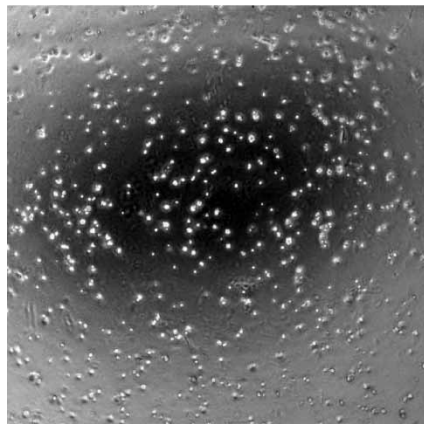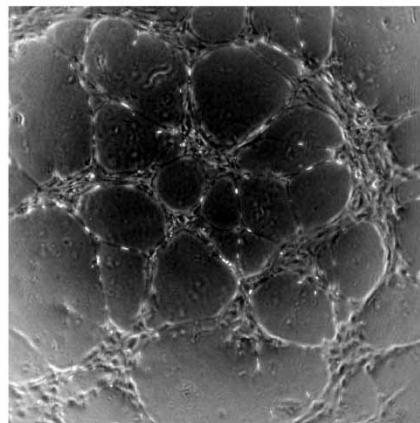

(a) $t = 0\,h$
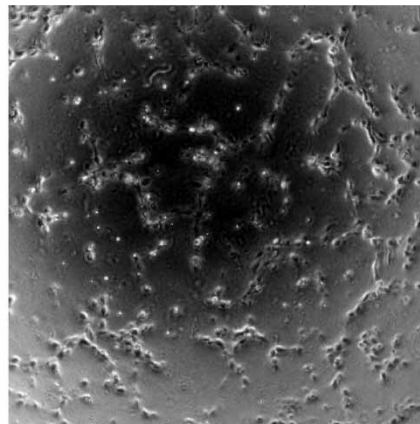
(b) $t = 3\,h$

(c) $t = 6\,h$

(d) $t = 9\,h$

Figure 1.   The process of formation of vascular networks. The visual field covers a portion of $2\,mm \times 2\,mm$ of Matrigel surface.

(iv) Finally, individual cells fold up to form the lumen of the capillary, so that one has the formation of a capillary-like network along the lines of the previously formed bidimensional structure as described in Kubota *et al.* [9] and Grant *et al.* [10].

It is important to notice that, since cells settle on a surface, one of the key parameters of the process is the density of cells per unit area (cells/mm^2). For this reason in the next section, we will we refer to this parameter and not the density of cells in the physiological solution (cells/ml), which is sometimes reported in the literature.

2.1 Cell trajectories at the early stage

If one focuses on the trajectory of a single cell it is easy to notice that in most cases the direction of motion is well established and maintained until the cells encounter other cells. Of course, a random component is present but is usually not predominant. The trajectory of an individual cell then shows *persistence* in the direction of motion, *i.e.*, the cell has a tendency to maintain its own direction of motion [21, 24] (figure 2). In most cases the motion is apparently directed toward zones of higher concentration of cells (see figure 2(a)). These two observations suggest respectively the presence of a mechanism of persistence in cell motion and a mechanism of cross-talk among cells. As a matter of fact, recent works [7, 25], confirm that endothelial cells (EC) in the process of vascular network formation exchange signals by the release and absorption of Vascular Endothelial Growth Factor (VEGF-A). This growth factor can bind to specific receptors on the cell surface and induce chemotactic motion along its concentration gradient [25]. Chemotactic cell movement is considered to be a key mechanism in several morphogenetic events, including vasculogenesis [27].

A good candidate as a soluble chemotactic mediator is VEGF-A, which is known to induce EC growth, survival, and motility [26, 28]. Moreover autocrine/paracrine secretion of VEGF-A by ECs has been shown to be essential for the formation of capillary beds [25]. As we shall see in the following section, addition of an anti-VEGF-A neutralizing antibody inhibits capillary network formation because it triggers EC apoptosis.

In order to quantify both cell persistence and the chemotactic behaviour in cell motion, Serini *et al.* [19] performed a statistical analysis of the cell trajectories on the basis of the cell displacement vectors over time intervals of one minute measured from videomicroscopic records.

They measured two angles, ϕ and θ (see figure 2(c)). The former is the angle between two subsequent displacements relative to the same trajectory. It then gives a measure of the persistence.

The latter is the angle between the velocities and the concentration gradients at the same point simulated starting from the distribution of cells and taking into account that VEGF-A, like similar soluble molecules, is degraded by the environment in a finite time, mainly through oxidation processes [29]. The angle θ then gives a measure of the chemotactic behaviour.

Figure 2(a,d,e) shows persistence of cell direction in time and alignment with the direction of simulated gradients of the concentration field in physiological conditions.

2.2 VEGF saturation or inhibition

In order to test the importance of chemotactic signaling mechanisms, Serini *et al.* [19] performed some experiments aimed at extinguishing VEGF-A165 gradients. Direct inhibition of VEGF-A caused an apoptotic effect. To overcome this problem, they extinguished VEGF-A gradients spreading from individual ECs plated of Matrigel by adding a saturating amount of exogenous VEGF-A165. Indeed, saturation of VEGF-A gradients resulted in strong inhibition of network formation. This observation is also confirmed in a set of experiments performed in the Boyden chamber and evaluated by checkerboard analysis to study the chemotactic and chemokinetic activity of VEGF-A165.

The same statistical analysis mentioned in the previous section was repeated in saturating conditions (figure 2(b)). In this case, the diagram for ϕ shows that cell movement maintains a certain degree of directional persistence, while the diagram for θ shows that in saturating conditions the movement is completely decorrelated from the direction of simulated VEGF gradients.

2.3 Chord length

The capillary-like network formed on Matrigel can be represented as a collection of nodes connected by chords. The mean chord length measured on the experimental records in Serini *et al.* [19] is approximately constant and equal to $\ell \simeq 200 \pm 20 \, \mu m$ over a range of values of seeded cell density n_0 extending from 100 to 200 cells/mm^2 (figure 3).

It is interesting to notice that capillary networks characterized by typical intercapillary distances ranging from 50 to 300 μm is instrumental for optimal metabolic exchange [4–6]. So the characteristic size of the network *in vitro* is biologically functional: a coarser net would cause necrosis of the tissues in the central region, a finer net would be useless.

A deeper analysis of the statistical distribution of chord length can be found in Ambrosi *et al.* [30] and Gamba *et al.* [31].

Ruhrberg *et al.* [32] observed that mice lacking heparin-binding isoforms of VEGF-A form vascular networks with a larger mesh (see figure 4). This is related to the fact that binding of some of the isoforms with lower or higher molecular weight affects the effective diffusivity of the chemical factor. Therefore VEGF plays a role in defining the mesh size and, in particular, different isoforms (with different diffusivities) can lead
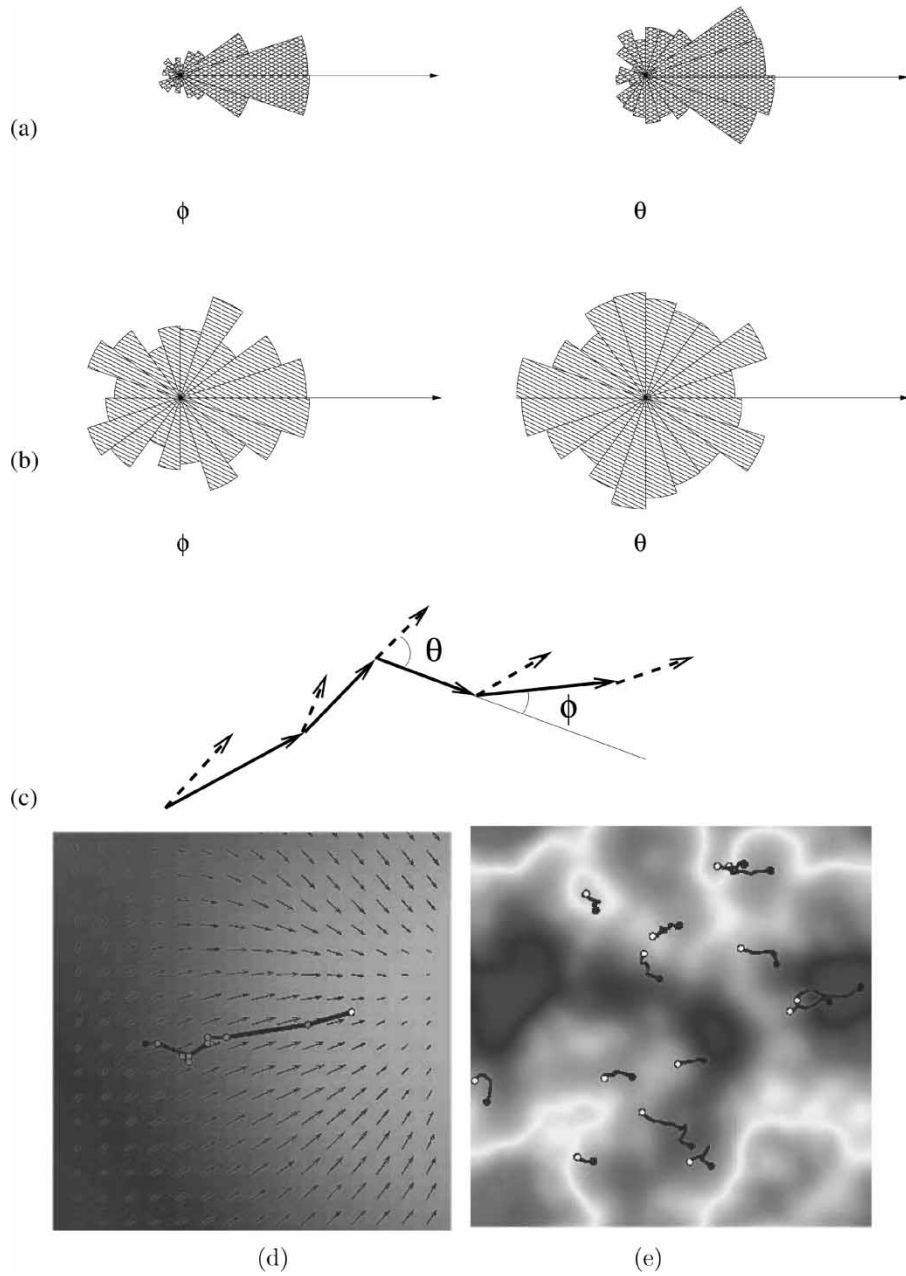
Figure 2. Rose diagram under (a) normal and (b) saturated conditions. The motion is correlated with the direction of the VEGF gradient in normal conditions and completely uncorrelated in saturating conditions. A marked persistence in cell motion is evident both in normal and in saturating conditions, though in the latter case the effect decreases. (c) Definition of the angles ϕ and θ referring respectively to persistence and chemotaxis. The dashed arrows refer to the local concentration gradient. (d) Trajectories of some cells under physiological conditions. (e) Sample trajectory in the field of chemoattractant. Again arrows indicate concentration gradients.

to different mesh size. As discussed in the sequel, the model by Gamba *et al.* [31] and Serini *et al.* [19] predicts that the size of the network is related to the product of the diffusion constant and the half-life of the chemical factor.

2.4 Dependence on cell density

If on one hand the chord length is nearly independent from the density n_0 of seeded cells in a certain range, on the other hand it is observed that outside this range one does

not have a proper development of vascular networks, as observed *in vivo* by Fong *et al.* [33]. To enlighten this phenomenon, Serini *et al.* [19] performed some experiments varying the density of seeded cells demonstrating the presence of a percolative-like transition [34] at small densities and a smooth transition to a "Swiss-cheese" configuration at large density.

In fact, below a critical value $n_c \sim 100 \, \text{cells/mm}^2$ the single connected network (figure 5(b)) breaks down in groups of disconnected structures (figure 5(a)). On the other hand at higher cell densities, say above
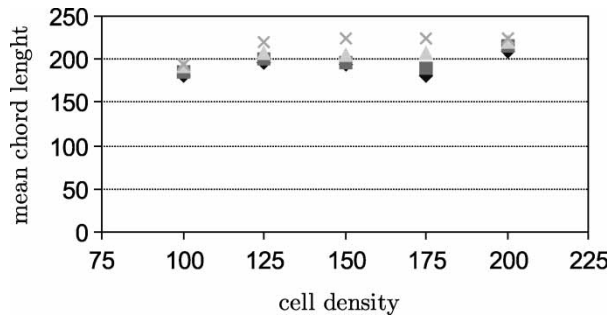
Figure 3. Mean values of chord lengths of network structures obtained varying initial cell densities and with cell samples taken from four different experiments.

$200 \, \text{cells/mm}^2$ (figure 5(d)), the mean chord thickness grows to accommodate an increasing number of cells.

For an even higher value of n_0, the network takes the configuration of a continuous carpet with holes (figure 5(d)). This configuration is not functional. In fact, cells do not even differentiate to form the lumen in the chords. Among other things, the paper by Tranqui and Traqui [20], which also focuses on the formation of lacunae, analyses the content of fibronectin in the substratum and finds that the holes are deprived of fibrin.

2.5 Stiffness of the substratum and protease inhibitors

Vailhé *et al.* [35] performed some experiments changing the fibrin concentration in a substratum of 1 mm thickness. They start with an initial condition in which cells are confluent and form a continuous carpet of cells (probably $n_0 \approx 1500 \, \text{cells/mm}^2$). Increasing the fibrin concentration from 0.5 mg/ml to 8 mg/ml, the number of lacunae formed by Human Umbilical Vein Endothelial Cells (HUVEC) strongly decreased, without increasing in size. In fact, capillary networks only formed for fibrin concentration of 0.5 mg/ml with a typical chord length of $550 \pm 50 \, \mu\text{m}$. At the extreme value of 8 mg/ml, the ensemble of cells represented a continuous carpet with no holes. An examination of their pictures suggests that, during the process, the cells undergo apoptosis or detach from the surface. In fact, the total mass does not seem to be conserved during the process. This may be due to the fact that fibrinolysis leads to cell detachment at the end of the process.

They repeated the experiments using Bovin Retinal Endothelial Cells (BREC), which required a fibrin concentration of 8 mg/ml to form capillary network and formed a structure with a mean chord length of $400 \, \mu\text{m}$. In fact, BREC presented a high fibrinolytic activity so that at lower concentration gels were degraded too quickly and the cells could not adhere. Adding aprotin at a concentration of $1 \, \mu\text{g/ml}$ decreased the degradation and allowed the formation of capillary-like structures.

Vailhé *et al.* [35] also noticed that the formation of lacunae was accompanied by a degradation of fibrin gels in the lacunae. They measured the fibrin degradation products present in the culture medium and found an increase after 10 hours of seeding the HUVEC.

For this reason some experiments were performed adding protease inhibitors (aprotin up to a concentration of $10^{-4} \, \mu\text{g/ml}$ for HUVEC). They never observed networks when the fibrin degradation had been completely inhibited. On the other hand, in some cases (e.g., fibrin concentration of 8 mg/ml) degradation was not sufficient to ensure the formation of capillary-like networks.

2.6 Effect of gel thickness

Many experiments performed by Vernon and coworkers focus on the interaction between cells and extracellular matrix (ECM). In particular, Vernon *et al.* [36, 37], and Sage [38] performed some experiments seeding Bovine Aorthic Endothelial Cells (BAEC), cells of the murine Leydig cell line TM3, human fibroblasts, human smooth muscle cells, and murine PYS-2 cells on gelled basement membrane matrix (BBM) of 1 mm thickness. The BMM was made more rigid by adding varying amounts of gelled native type I collagen. In particular, with 0.6 mg/ml collagen, BAEC and TM3 cells formed capillary networks in 24 h. On the other hand, increasing the amount of collagen to 2 mg/ml resulted in cells that were flattened, spread, and unorganized.

In addition, they used a set-up in which the substratum was distributed with a triangular shape increasing from 10 to 500 μm over a length of 17 mm, or from 10 to 400 μm over a length of 4 mm. (For comparison the thickness used in the experiments by Serini *et al.* [19] correspond to 7% of the slope length of the experiment on the thinnest side.) The experiment shows the formation of longer chords where the thickness is higher and shorter chords where it is

Figure 4. Dependence of chord length from VEGF effective diffusivity (adapted from [32]).

(a) $n_0 = 62.5$

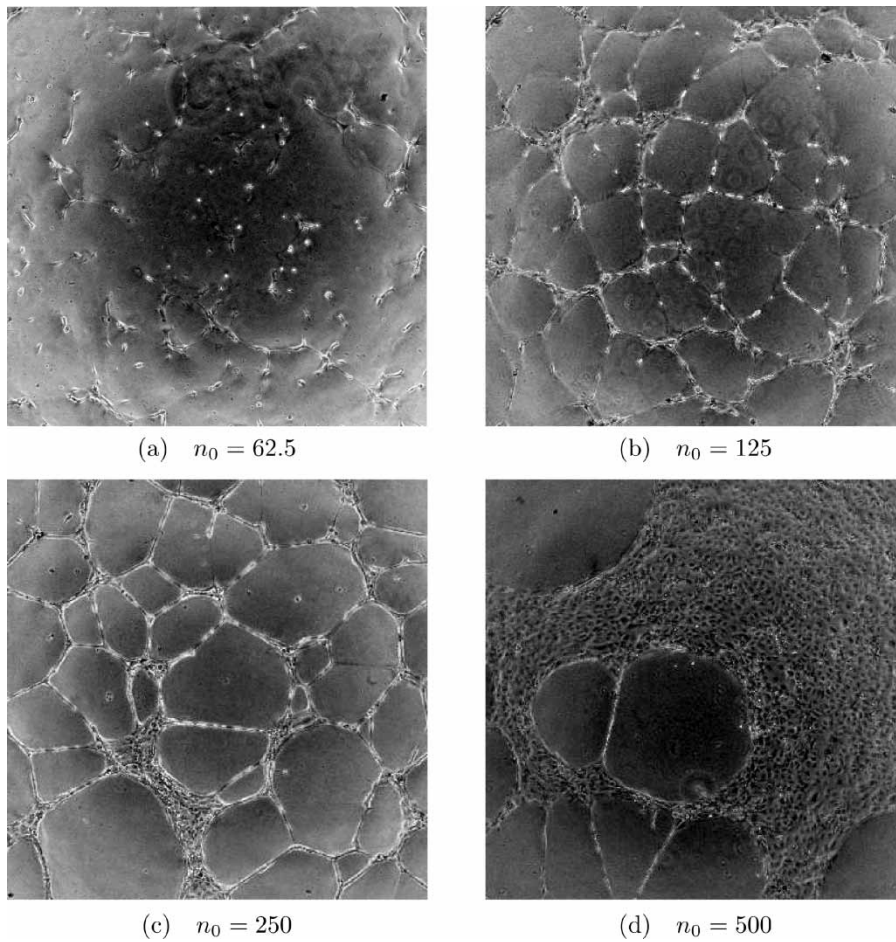(b) $n_0 = 125$

(c) $n_0 = 250$

(d) $n_0 = 500$

Figure 5.   Dependence of the types of structures formed varying the density of seeded cells.

lower. Where the substratum is too thin there is probably no capillary structure at all.

3. How persistence and endogenous chemotaxis drive capillary network formation

The work by Gamba *et al.* [31] and Serini *et al.* [19] focuses on the early development of vascular network formation. Their basic assumption is that persistence and chemotaxis are the key features determining the size of the structure. In their view, mechanical interaction of the cells with the Matrigel can be neglected for describing the behaviour of the system along the first 3 to 6 hours.

Their mathematical model is based on the following assumptions:

(1) Endothelial cells show persistence in their motion.
(2) Endothelial cells communicate via the release and absorption of molecules of a soluble growth factor.
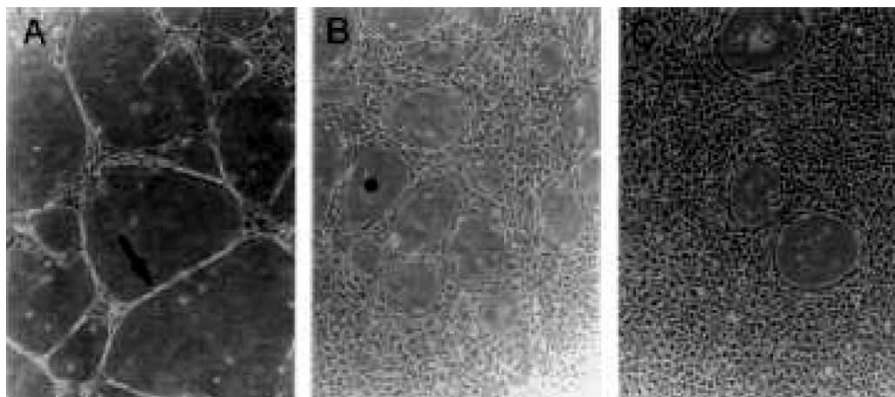

Figure 6.   Formation of lacunae and capillary networks at different fibrin concentrations, 0.5, 2 and 4 mg/ml (adapted from [20]).

This chemical factor can be reasonably identified with VEGF-A [19].

(3) The chemical factors released by cells diffuse and degrade in time.

(4) Endothelial cells neither duplicate nor die during the process.

(5) Cells are slowed down by friction due to the interaction with the fixed substratum.

(6) Closely packed cells mechanically respond to avoid overcrowding.

The following state variables are introduced:

- The density n of endothelial cells,
- The velocity $\mathbf{v}$ of the endothelial cells,
- The density c of chemoattractant.

The mathematical model then writes as

$$\frac{\partial n}{\partial t} + \nabla \cdot (n\mathbf{v}) = 0, \tag{1}$$

$$\frac{\partial (n\mathbf{v})}{\partial t} + \nabla \cdot (n\mathbf{v} \otimes \mathbf{v}) = \mathbf{f}, \tag{2}$$

$$\frac{\partial c}{\partial t} = D\Delta c + \alpha n - \frac{1}{\tau}c. \tag{3}$$

Equation (1) is a mass conservation equation corresponding to the assumption that cells do not undergo mitosis or apoptosis during the experimental phenomenon. Equation (3) is a diffusion equation for the chemical factor which is produced at a rate α and degrades with a half life τ.

Equation (2) assumes that cell motion can be obtained on the basis of a suitable force balance. Although the second term at the L.H.S. of the momentum equation reminds the convective flux of cellular matter, it should be understood as a term modeling cell persistence; their "inertia" in changing cell direction. The "force" $\mathbf{f}$ then models the reasons which may cause a change in cell persistence. These include

(1) A chemotactic body force

$$\mathbf{f}_{\text{chem}} = \beta n \nabla c \tag{4}$$

where β measures the intensity of cell response per unit mass. The linear dependence on n corresponds to the assumption that each cell experiences a similar chemotactic action. Of course, a saturation effect on the amount of chemoattractant could be included, for instance in order to model the phenomena described in section 2.2. The generalization of the model to the case of multiple species of chemical factors, characterized by different physical properties and biological actions (e.g. attraction and repulsion), is also of interest to understand how to govern the formation of the network, and will be discussed in the final section.

(2) A dissipative interaction with the substrate

$$\mathbf{f}_{\text{diss}} = -\gamma n \mathbf{v}. \tag{5}$$

The linear dependence of $\mathbf{f}_{\text{diss}}$ on n corresponds to the assumption that each cell is subject to the same dissipative forces.

(3) The incompenetrability of cellular matter, to model the fact that closely packed cells resist to compression

$$\mathbf{f}_{\text{surf}} = -\nabla[n\pi(n)]. \tag{6}$$

After some standard algebra, equations (1)–(3) rewrite

$$\frac{\partial n}{\partial t} + \nabla \cdot (n\mathbf{v}) = 0, \tag{7}$$

$$\frac{\partial \mathbf{v}}{\partial t} + \mathbf{v} \cdot \nabla \mathbf{v} = \beta \nabla c - \gamma \mathbf{v} - \nabla \varphi(n), \tag{8}$$

$$\frac{\partial c}{\partial t} = D\Delta c + \alpha n - \frac{c}{\tau}, \tag{9}$$

where $\varphi(n)$ is defined by

$$n\frac{\mathrm{d}\varphi}{\mathrm{d}n} = \frac{\mathrm{d}}{\mathrm{d}n}(n\pi), \tag{10}$$

or

$$\varphi = \int \frac{1}{n}\frac{\mathrm{d}}{\mathrm{d}n}(n\pi)\mathrm{d}n. \tag{11}$$

For quick reference, in the following we will refer to equations (7)–(9) as the PEC model (Persistence and Endogenous Chemotaxis).

Notice that dropping the pressure and persistence terms in equation (8), an assumption that corresponds the immediate adjustment of the cells to the limit velocity, leads to classical chemotactic models [39, 40], for which blow-up in finite time is possible. The important feature of the function $\varphi(n)$ in the qualitative analysis and in the simulation is that it must vanish below the close-packing density N and then rapidly increase above it. When preserving the pressure term, one has the model studied by Kowalczyk [41] in which the blow-up of the solution is prevented under suitable characterization of the pressure-density dependence. To this aim, a sufficient condition is that the function $\varphi(n)$ grows faster than a logarithm for high cell densities, i.e.

$$\frac{\mathrm{d}\varphi}{\mathrm{d}n} > \frac{C}{n}, \quad \text{for large } n.$$

By a Chapman-Eskog expansion Filbet *et al.* [42] derive the model (1)–(3) as a hydrodynamic limit of a kinetic velocity-jump process. They also performed simulations

obtaining results similar to those shown in figure 7 and discussed in the following section.

3.1 Qualitative analysis and numerical simulations

The experiments described in the section above start with a number of cells randomly seeded on the Matrigel. To reproduce the experimental initial conditions Gamba *et al.* [31] and Serini *et al.* [19] integrate numerically equations (7)–(9) with the following initial conditions:

$$n(\mathbf{x}, t = 0) = \frac{1}{2\pi r^2} \sum_{j=1}^{M} \exp\left[-\frac{(\mathbf{x} - \mathbf{x}_j(\omega))^2}{2r^2}\right], \qquad (12)$$

$$\mathbf{v}(\mathbf{x}, t = 0) = 0. \qquad (13)$$

This choice corresponds to a collection of *M* Gaussian bumps in cell density; their width is of the order of the average cell radius $r \simeq 20\,\mu m$ and they are centered at random locations $\mathbf{x}_j$ distributed with uniform probability on a square of size *L*. The initial velocity is null and periodicity is imposed at the boundary of the domain.

The results of the simulations are shown in figure 7. Figure 8 shows how the precise network structure depends on the initial conditions which are randomly set. However, the general features seem to be independent on the precise form of the initial condition and compare well with the experimental results shown in figure 1.

Let us now consider the information encoded in the coupling of the continuum model (7) and (8) with the diffusion equation (9). This can be understood in the simplest way if we neglect pressure and assume that diffusion is a faster process than pattern formation, so that the dynamics of *c* is "slaved" to the dynamics of *n* and the derivative term $\partial c/\partial t$ can be neglected in a first approximation. Then it is possible to solve equation (9) formally for *c* and to substitute in equation (8), thus obtaining
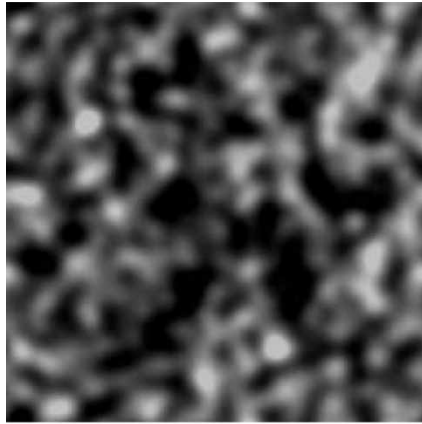
$$\frac{\partial \mathbf{v}}{\partial t} + (\mathbf{v}\cdot\nabla)\mathbf{v} = \frac{\alpha\beta}{D}\nabla(\ell^{-2} - \Delta)^{-1}n. \qquad (14)$$

The appearance in the dynamical equations of the characteristic length

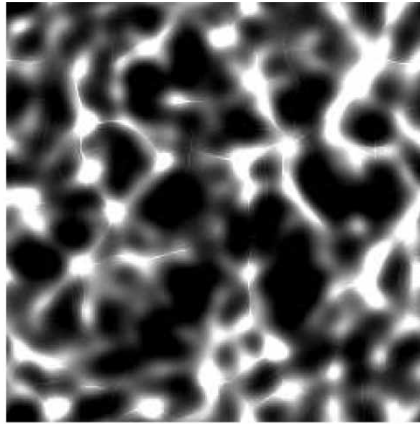$$\ell =: \sqrt{D\tau}, \qquad (15)$$

suggests that the dynamics could favour patterns characterized by this length scale. As a matter of fact, if we rewrite the R.H.S. of equation (14) in Fourier space as
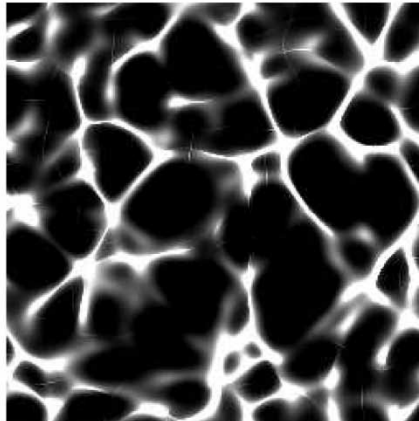
$$\frac{\alpha\beta}{D}\frac{i\mathbf{k}}{k^2 + \ell^{-2}}n_{\mathbf{k}},$$

(a) $t = 0$

(b) $t = 3\,h$

(c) $t = 6h$

Figure 7.   (a−c) Simulation of the initial development of vascular networks.
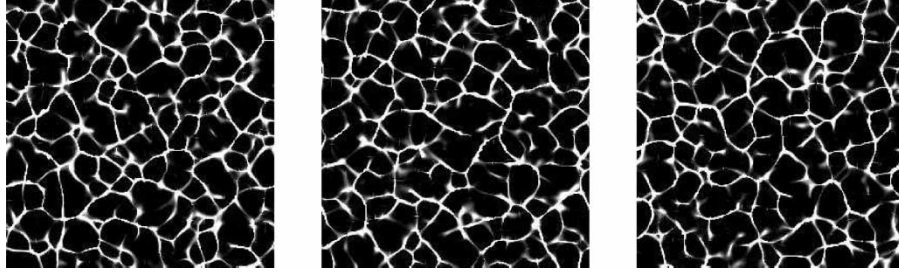
Figure 8.   Dependence of the specific network structure on the initial conditions.

we observe that the operator $\mathbf{i}\mathbf{k}/(k^2 + \ell^{-2})$ acts as a filter, which selects the Fourier components of n having wave numbers of order ℓ^{-2} damping the components with higher and smaller wavenumbers.

The diffusion coefficient can be estimated from available data of molecular radii [43, 44] using the Einstein–Stokes relation $D = k_B T/(6\pi\eta r_H)$ where k_B is the Boltzmann's constant, T the temperature, η the solvent viscosity, r_H is the hydrodynamic radius of the molecule [45]). In the case of VEGF-A, this gives $D \sim 10^{-7}\,\mathrm{cm}^2\,\mathrm{s}^{-1}$.

The other key parameter involved in the identification of the characteristic length scale is the half-life of VEGF-A, which was measured by Serini *et al.* [19] in their experimental setting using a radioactive tracer, giving the value $\tau = 64 \pm 7\,\mathrm{min}$.

This gives $\ell \sim 100\,\mu\mathrm{m}$, which is in good agreement with experimental data.

The process of network formation is then understood in the following way. Initially, non-zero velocities are built up by the chemoattractive term due to the presence of random inhomogeneities in the density distribution. Density inhomogeneities are translated in a landscape of concentration of the chemoattractant factor where details of scales ℓ are averaged out. The cellular matter moves towards the ridges of the concentration landscape. A non-linear dynamical mechanism similar to that encountered in fluid dynamics sharpens the ridges and empties the valleys in the concentration landscape, eventually producing a network structure characterized by a length scale of order ℓ. In this way, the model provides a direct link between the range of intercellular interaction and the dimensions of the structure which is a physiologically relevant feature of real vascular networks.

Intriguingly, this seems in agreement with the observation that mice lacking heparin-binding isoforms of VEGF-A, characterized by larger effective diffusivity, form vascular networks with a larger mesh (see [32] and figure 4). Although the vascular patterns observed *in vivo* in Ruhrberg *et al.* [32] are mainly thought to be generated by angiogenesis rather than vasculogenesis, one cannot exclude the possibility of a simultaneous occurrence of both phenomena [46]. Figure 9 shows for comparison the results of some simulations obtained increasing the characteristic length.

It can be observed that scaling lengths with ℓ, times with $T = \sqrt{D/\alpha\beta N}$, cell density in units of the close-packing density N (confluent distribution), and VEGF concentration with $C = \alpha t N$ (i.e., a measure of the amount of soluble factor produced by a close packing density of cell during time τ), the dimensionless model presents very few dimensionless parameters. One multiplies the L.H.S. of the diffusion equation and is known to be very small. Another multiplies the drag term, which appears to influence the simulation very weakly. As we shall see in the following sections, the important dimensionless parameter is contained in the initial condition and compares the initial density with the close packing one. Then the geometry of patterns essentially depends only on D and τ while the parameters α and β influence the time needed for the structure to form. In fact, they are related to VEGF production and chemotactic response by endothelial cells.

3.2 Percolative transition

In the previous section, it is discussed how the model is able to foresee the exact dynamics starting from realistic initial data which mimic a set of randomly seeded cells initially at rest. This section and the following one will focus on the dependence of the characteristics of the structure on the density of seeded cells and, in particular, on the transitions occurring at small and large densities, respectively (compare figures 5 and 10). The results of the simulations are in remarkable agreement with the experiments. By varying the initial number of cells one switches from a phase in which dynamics generate several disconnected structures to a phase in which a single connected structure appears. This process is an example of percolative transition (figure 11).

The concept of percolation has been used in statistical mechanics to describe the formation of connected clusters of randomly occupied sites in systems close to critical values of the parameters. By varying the occupation probability in infinite systems one observes a phase transition in which the probability of percolating over a connected cluster extending across the whole system suddenly jumps from 0 to 1 [34]. Percolative transitions have been thoroughly investigated and are classified in a small number of "universality classes", characterized by scaling laws with well defined "critical exponents".
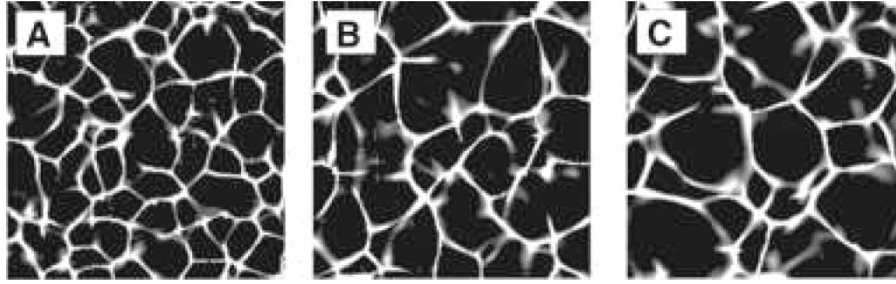
Figure 9. Dependence of the network characteristic size on $\ell = 100, 200, 300\,\mu$m.

These exponents are fingerprints of the growth process that led to vascular structure formation and it has been suggested that they may help to discriminate between healthy and pathological structures [47].

Methods of statistical mechanics were used in Gamba *et al.* [31] to characterize quantitatively the sharp percolative transition. Its presence in the process of formation of vascular networks is not obvious, and is linked to the average constancy of the chord length. As a matter of fact, there are at least two ways of accommodating an increasing number of cells on a vascular-type network. The first one is to force side-to-side connectivity allowing arbitrary chord lengths as in figure 11(a). The second one is to enforce the constraint on the chord length. In this case, when the number of cells is too low side-to-side connectivity cannot be achieved and one only has sets of disconnected clusters as in figure 11(a).

It appears that Nature in this case chose the second way because widely spaced capillary networks, like the one on the left of figure 11(a), would not be able to perform their main function, i.e. to supply oxygen and nutrients to the central part of the tissues [6]. This confirms that there must exist a precise mechanism controlling the average chord length during vascular formation, like the one hypothesized in the deduction of model (1)–(3).

Gamba *et al.* [31] and Coniglio *et al.* [48] performed a detailed analysis of the type of percolative transition which is observed, finding that from both experiments and

(a) $n_0 = 62.5$

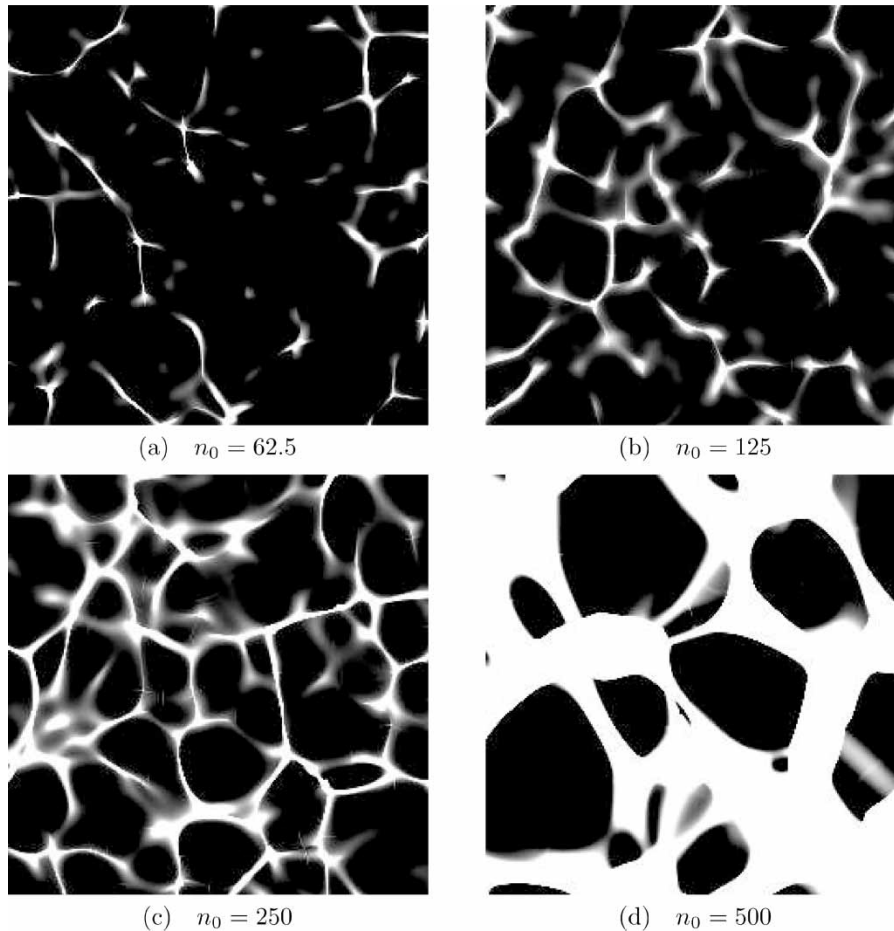(b) $n_0 = 125$

(c) $n_0 = 250$

(d) $n_0 = 500$

Figure 10. Simulation of the dependence of the types of structures formed varying the density of cells.

simulations it occurs in the neighbourhood of $n_c \sim 100$ cells/mm^2. They also concluded that the transition falls in the universality class of random percolation, even in the presence of migration and dynamical aggregation. This is confirmed by the fractal dimension of the percolating cluster. In fact, as shown in figure 11(e), on scales larger than $r_c \approx 0.8$ mm, both the value obtained on the basis of the experiments ($D = 1.85 \pm 0.10$) and that obtained on the basis of the numerical simulations ($D = 1.87 \pm 0.03$) are close to the theoretical value expected for random percolation ($D = 1.896$). Another interesting characteristic of the capillary network structure is given by a bi-fractal behaviour. In fact, if observed at a scale smaller than r_c the vascular network shows a different scaling behaviour characterized by a fractal dimension of $D \approx 1.50 \pm 0.02$ both on the basis of experiments and simulations. According to Gamba *et al.* [31] this might be the signature of the dynamical process that led to the formation of the network.

3.3 "Swiss-cheese" transition

The same mechanism schematized in the previous section and sketched in the cartoon in figure 11(b−d) might in principle also explain the formation of lacunae. If the number of cells doubles, there are two ways of accommodating the new cells. Either placing them in a more homogeneous way, forming smaller squares, as on the left of figure 11(c), or addensing the new cells next to the others, as on the right of figure 11(c). In the first case the size of the squares halves, in the second case it remains

nearly the same, but the chords thicken. It seems that, for the same reason explained in the percolative transition, Nature prefers to keep the size of the network as far as possible. Eventually, this leads to the formation of lacunae as on the right of figure 11(d).

In order to study the formation of lacunae starting from a continuous monolayer of cells (using the words in Serini *et al.* [19], the "Swiss-cheese" transition, see also figure 5(d)) Kowalczyk *et al.* [49] studied the linear stability properties of the model (7)–(9) (they also considered the presence of a non crucial viscous term).

They found that if $\varphi'(n_0) > \alpha\beta\tau$ then the uniform solution with cell density n_0 is linearly stable. At criticality instability starts as a long wave instability. Assuming φ to be a convex function the criterium above means that the system is unstable at low densities and stabilizes at higher densities (close packing densities), in agreement with the experiments.

Decreasing even further the density of cells, the critical wave number increases and becomes infinite in the limit of "very small" $\varphi'(n_0)$.

The PEC model then describes the dynamics of the generation of lacunae as follows: Chemotaxis with the related parameters (motion, production and degradation) is the key destabilizing force, while pressure is the main stabilizing force.

In fact, the presence of the pressure term is crucial since it avoids overcompression in the chords and also allows to reproduce the transition to the "Swiss-cheese" regime that is experimentally observed for $n_0 > 300$ cells/mm^2 (figure 5(d)).
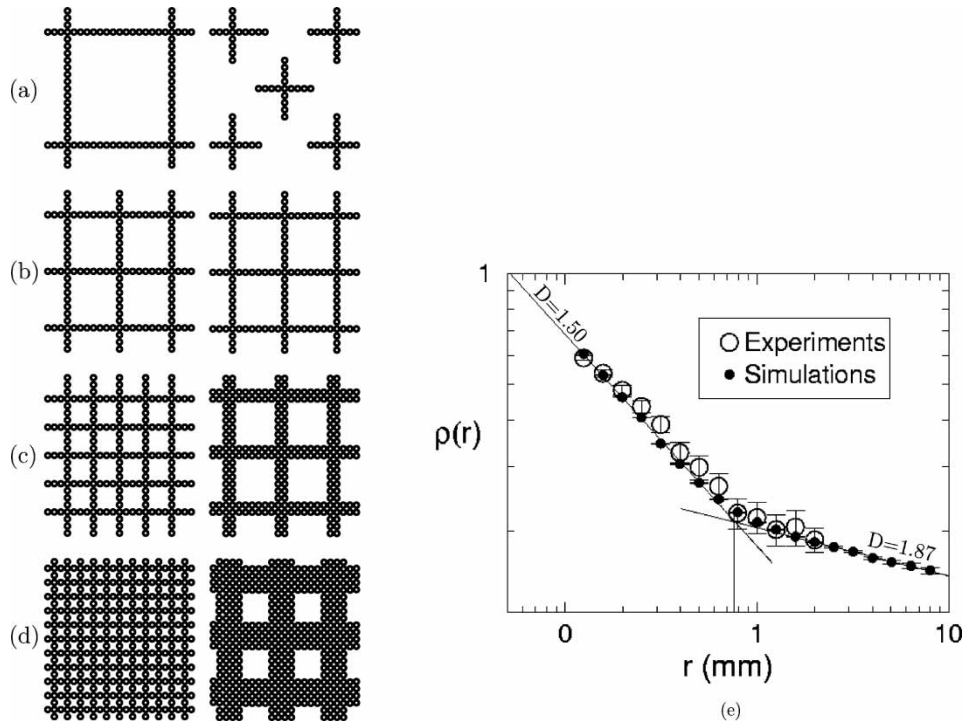

Figure 11.   (a−d) Cartoon relative to the percolative transition. (e) Density of the percolating cluster ($\rho(r) \approx r^{D-2}$ where D is the fractal dimension) as a function of the radius for numerical simulation and experimental data.

4. Cell traction and capillary network formation

Mechanical models aimed at describing the formation of capillary network were developed in the last decade after the pioneering paper by Murray, Oster, and Harris [50], which was mainly devoted to mesenchymal morphogenesis on the basis of experiments by Harris, Stopak, and Wild [51] on the interaction between ECM and fibroblasts, a type of cell well known for its strong pulling force. This paper (and also [52–54]) modelled the interactions between a cell population and the ECM substratum they move in, placing special emphasis on the morphogenic role played by cellular traction forces.

The essential features of the models developed on this basis to deal with vasculogenesis are as follows:

1. Cells exert traction forces on to the ECM, which is a viscoelastic material;
2. The Petri dish exerts a drag force on the matrix;
3. Possibly cells move because of haptotaxis or chemotaxis.

The following state variables are considered:

- The density n of endothelial cells;
- The density ρ of ECM;
- The displacement $\mathbf{u}$ of ECM from its original position.

All the mathematical models inspired by the seminal paper of Murray and co-workers can be written in the following form:

$$\frac{\partial n}{\partial t} + \nabla \cdot \mathbf{J} = \Gamma, \tag{16}$$

$$\frac{\partial \rho}{\partial t} + \nabla \cdot (\rho \mathbf{w}) = -\Delta, \tag{17}$$

$$-\nabla \cdot \mathbf{T}_n - \nabla \cdot \mathbf{T}_\rho = \mathbf{F}, \tag{18}$$

where $\mathbf{w} = \mathrm{d}\mathbf{u}/\mathrm{d}t$ is the ECM velocity, $\mathbf{J}$ is the cellular flux, Γ refers to the (possible) generation and death of cells, Δ is the (possible) digestion of ECM by the cells, $\mathbf{T}_n$ is called "cell traction stress" and $\mathbf{T}_\rho$ is the stress in the deformed ECM. Finally, $\mathbf{F}$ is the force due to the interaction between the ECM and the Petri dish.

Equations (16) and (17) are mass balance equations. In principle, cells might duplicate or die during the process and ECM is degraded and produced by the cells. However, as already stated in the previous section, in the time needed for the pattern to form, both cell duplication/apoptosis and ECM production/degradation can be neglected, so that in most cases equations (16) and (17) write as conservation equations. Only Manoussaki [55] introduces a growth term on the R.H.S. of equation (16) but then neglects it in the stability analysis and in the simulation. Conversely, Tranqui and Traqui [20] consider

ECM degradation claiming that it plays a role in the formation of lacunae.

The last equation is a force balance equation for the whole system, the mixture of cells and Matrigel. The term $\mathbf{T}_n$ accounts for the forces internal to the system due to the cell traction, $\mathbf{T}_\rho$ accounts for the elastic response of the matrix.

For quick reference in the following we refer to equations (16)–(18) as "elasto-mechanical model".

Entering more in detail, four types of contributions can be identified in the cellular flux $\mathbf{J}$

- A passive motion due to the attachment of the cells on the moving ECM, $\mathbf{J}_w = n\mathbf{w}$;
- A strain dependent motion $\mathbf{J}_d = -\nabla \cdot [D(\mathbf{I} + \mathrm{dev}(\mathbf{E}))n]$, where

$$\mathrm{dev}(\mathbf{E}) = \mathbf{E} - \frac{\mathrm{tr}\mathbf{E}}{2}\mathbf{I} \tag{19}$$

and

$$\mathbf{E} = 1/2(\nabla \mathbf{u} + \nabla \mathbf{u}^T)$$

is the strain tensor and $\mathrm{tr}\,\mathbf{E} = E_{xx} + E_{yy}$;

- A haptotactic motion along the adhesive ECM density gradients $\mathbf{J}_\rho = kn\nabla\rho$;
- A chemotactic motion along the gradients of a specific chemical factor c, $\mathbf{J}_c = \chi n\nabla c$.

The first two contributions are always present, while haptotaxis is considered in Tranqui and Traqui [20] and Namy *et al.* [56] and chemotaxis in Manoussaki [55].

The cell traction stress is always taken to be isotropic through a density dependent function, i.e. $\mathbf{T}_n = \Sigma_n(n)\mathbf{I}$ where $\mathbf{I}$ is the identity tensor. Manoussaki *et al.* [57], Murray *et al.* [58], Manoussaki [55], and also Murray and Swanson [59] and Murray [60] propose the following form

$$\Sigma(n) = \tau \frac{n}{1 + \alpha n^2}, \tag{20}$$

which grows linearly for low cell densities and, after reaching a maximum at $n = 1/\sqrt{\alpha}$, goes to zero for large densities, corresponding to what the Authors call a saturation effect due to the fact that at high densities not all cells are able to pull. There is then an upper limit to the pulling force possible.

Tranqui and Traqui [20] and Namy *et al.* [56] propose

$$\Sigma(n) = \hat{\tau}\rho n(N - n), \tag{21}$$

which has a similar behaviour for small densities with a maximum at $n = N/2$, but becomes negative for $n > N$

corresponding to "cell pushing" at high densities. That is, while (20) is always an attractive force, (21) leads to cell repulsion at sufficiently high cell density. The role of the repulsion is similar to the pressure term in the PEC models.

Though deformations are not small, ECM is usually described as a linear Voigt-Kelvin material

$$\mathbf{T}_{VK} = \frac{E}{1+\nu}\left(\mathbf{E} + \frac{\nu}{1-2\nu}\mathrm{tr}(\mathbf{E})\mathbf{I}\right) + \mu_1\frac{\partial\mathbf{E}}{\partial t}$$
$$+ \mu_2\frac{\partial\mathrm{tr}(\mathbf{E})}{\partial t}\mathbf{I}, \qquad (22)$$

where $\mathbf{I}$ is the identity matrix, ν is the Poisson ratio, E is the Young modulus, μ_1 and μ_2 are the shear and bulk viscosities. Kowalczyk *et al.* [49] treated the ECM as a standard linear solid which satisfies the constitutive equation

$$\Lambda\frac{\partial\mathbf{T}_\rho}{\partial t} + \mathbf{T}_\rho = \frac{E}{1+\nu}\left(\mathbf{E} + \frac{\nu}{1-2\nu}\mathrm{tr}(\mathbf{E})\mathbf{I}\right) + \mu_1\frac{\partial\mathbf{E}}{\partial t}$$
$$+ \mu_2\frac{\partial\mathrm{tr}(\mathbf{E})}{\partial t}\mathbf{I}. \qquad (23)$$

On the other hand, Tranqui and Traqui [20] and Namy *et al.* [56] also considered long-range effects related to the fibrous nature of the ECM

$$\mathbf{T} = \mathbf{T}_{VK} + \mathbf{T}_L, \quad \text{with}$$

$$\mathbf{T}_L = -\frac{E}{1+\nu}\left(\beta_1\nabla^2\mathbf{E} + \frac{\nu}{1-2\nu}\beta_2\nabla^2\mathrm{tr}(\mathbf{E})\mathbf{I}\right). \quad (24)$$

The possibility of the existence of such a contribution was also mentioned in Murray and Swanson [59].

Finally, the anchoring force $\mathbf{F}$ is either modelled as an elastic force

$$\mathbf{F} = -\frac{\hat{s}}{\rho}\mathbf{u}, \qquad (25)$$

[20, 56], or as a viscous drag force

$$\mathbf{F} = -\frac{s}{\rho}\mathbf{w}, \quad \text{or} \quad \mathbf{F} = -\frac{s}{h}\mathbf{w}. \qquad (26)$$

The length h is the substratum thickness at rest [55, 57–61] and is related to the ECM density through $\rho = \hat{\rho}h$, because the ECM volumetric density $\hat{\rho}$ (i.e. kg/mm^3) does not change.

Kowalczyk *et al.* [49] considered a general dependence on the matrix density

$$\mathbf{F} = -\frac{s}{f(\rho)}\mathbf{w}. \qquad (27)$$

Taking the above assumptions into account the model (16)–(18) can be rewritten as

$$\frac{\partial n}{\partial t} + \nabla\cdot(n\mathbf{w}) = \nabla\cdot\nabla\cdot[\mathbf{D}(\mathbf{E})n] - \nabla\cdot\mathbf{J}_{ch} + \Gamma, \qquad (28)$$

$$\frac{\partial\rho}{\partial t} + \nabla\cdot(\rho\mathbf{w}) = -\Delta, \qquad (29)$$

$$\nabla\Sigma_n(n) - \nabla\cdot\mathbf{T}_\rho = \mathbf{F}, \qquad (30)$$

where $\mathbf{J}_{ch} = \mathbf{J}_c + \mathbf{J}_h$. Tables 1 and 2 summarize the forms of the terms used in the different papers.

Sometimes the mass balance equation (29) for the ECM is substituted with an equation relating the density ρ with the dilatation. This is obtained joining the mass balance equation in Lagrangian coordinates ($\rho_0 = \rho\det(\mathbf{I} + \nabla\mathbf{u})$) and the z-component of the stress balance. Slightly different formula can be found in the literature, due to the approximation and the definition of $\mathrm{tr}(\mathbf{E})$ introduced. For instance, following Namy *et al.* [56] one has

$$\rho = \rho_0\left(1 - \frac{\nu}{1-\nu}\mathrm{tr}(\mathbf{E})\right), \qquad (31)$$

and one can relate the thickness of the layer to the density of the gel through

$$h = h_0\left(\frac{1-3\nu}{1-2\nu} + \frac{\nu}{1-\nu}\frac{\rho}{\rho_0}\right). \qquad (32)$$

On the other hand, having in mind the application of the mechanical model to angiogenesis, Holmes and Sleeman [61] replace equation (29) with the reaction diffusion equation

$$\frac{\partial\rho}{\partial t} = D_\rho\nabla^2\rho + \frac{\varepsilon\rho n}{B+\rho} - \eta\rho n - \lambda\rho, \qquad (33)$$

Table 1. In the table VK stands for Voigt-Kelvin, VKL for Voigt-Kelvin with long range effects, SLS for standard linear solid, h refers to the thickness of the gel, E for "anisotropic pulling" $\mathbf{D} = \mathbf{D}(\mathbf{E})$, and D for "isotrophic pulling" $\mathbf{D} = D\mathbf{I}$.

Reference	D	Σ_n	$\mathbf{T}_\rho$	$\mathbf{F}_d$	ECM eq.
Manoussaki *et al.* [57]	E	$\frac{\tau n}{1+\alpha n^2}$	VK	$-\frac{s}{\rho}w$	(29)
Murray *et al.* [58] Murray and Swanson [59] Murray [60]	E	$\frac{\tau n}{1+\alpha n^2}$	VK	$-\frac{s}{h}w$	(31)
Manoussaki [55]	E	$\frac{\tau n}{1+\alpha n^2}$	VK	$-\frac{s}{h}w$	(29)
Holmes and Sleeman [61]	E	$\frac{\tau n}{1+\alpha n^2}$	VK	$-\frac{s}{\rho}w$	(33)
Levine *et al.* [62]					
Tranqui and Traqui [20]	D	$\hat{\tau}\rho n(N-n)$	VKL	$-\frac{\hat{s}}{\rho}u$	(29)
Namy *et al.* [55]	E	$\hat{\tau}\rho n(N-n)$	VKL	$-\frac{\hat{s}}{\rho}u$	(32)
Kowalczyk *et al.* [49]	D	$\tau\Sigma(n)$	SLS	$-\frac{\hat{s}}{f(\rho)}w$	(29)

Table 2. Summary of the terms used in the mass balance equations.

Reference	$\mathbf{J}_{ch}$	Γ	Δ
Manoussaki [55]	$\chi(c)n\nabla c$	γn	0
Tranqui and Traqui [20]	$kn\nabla\rho$	0	$\delta n\rho(N_1 - n)$
Namy *et al.* [55]	$kn\nabla\rho$	0	0
Holmes and Sleeman [61]	$\chi(c)n\nabla c + kn\nabla\rho$	$\gamma(c)n\left(1 - \frac{n}{N}\right)$	$-\frac{\varepsilon\rho n}{B+\rho} + n\rho n + \lambda\rho$

The other papers cited in table 1 do not include such terms.

which also considers the production and digestion of ECM by the endothelial cells.

The chemotactic effects introduced by Holmes and Sleeman [61] and Manoussaki [55] call for an equation describing the evolution of the concentration of tumour angiogenic factors (TAF)

$$\frac{\partial c}{\partial t} = D\nabla^2 c - \frac{Qcn}{N_n + c} + \alpha n. \quad (34)$$

As the simulations relative to both models aims at the description of angiogenesis, rather than vasculogenesis, TAF production is exogenous. For instance in Holmes and Sleeman [61], it is produced at the border of the domain where a non-growing tumour is assumed to grow.

4.1 Linear stability analysis

Most of the papers mentioned above perform a linear stability analysis of the solution of the elastomechanical model corresponding to the uniform distribution

$$n = n_0, \quad \rho = \rho_0, \quad \mathbf{u} = 0. \quad (35)$$

In our opinion, this analysis refers more properly to the formation of lacunae starting from a confluent distribution of cells, rather than phenomena involving a moderate density of aggregating cells. In fact, when seeding few cells the initial configuration is far from being a uniform distribution [56]. Of course, from a mathematical viewpoint it is always possible to start with a uniform density, but this is not the initial condition of most experiments dealing with vasculogenesis described in section 2.

According to the linear stability analysis of the elastomechanical model [55, 57], instability occurs if $n_0 < 1/\sqrt{\alpha}$ and

$$\frac{\tau}{E} > \left[\frac{1 - \nu}{(1 + \nu)(1 - 2\nu)} + \frac{sD_0}{Eh_0}\right]\frac{1}{n_0}\frac{(1 + \alpha n_0^2)^2}{1 - \alpha n_0^2}. \quad (36)$$

The result is also independent on whether the model includes a mass balance equation for the ECM, like for instance in Manoussaki *et al.* [57], or an equation like (31), as in Murray [58].

Therefore, for a given density of cells instability (and pattern formation) occurs only if the traction forces are sufficiently high or if the substratum is not too stiff.

The other interesting feature to examine is how the stability character of the solution depends on the density of cells. If one neglects saturation in the elasto-mechanical models by Murray *et al.* [58], Manoussaki *et al.* [57], Murray and Swanson [59], Murray [60] and Manoussaki [55], i.e. $\alpha = 0$, or, equivalently, $T_c = \tau n\mathbf{I}$, one has instability if

$$n_0 > \left[\frac{1 - \nu}{(1 + \nu)(1 - 2\nu)} + \frac{sD_0}{Eh_0}\right]\frac{E}{\tau}, \quad (37)$$

i.e. it is necessary to have a sufficiently high number of cells to trigger the formation of patterns, otherwise the uniform distribution is stable.

The physical explanation of the phenomenon is then the following: cells pull on the ECM. If the cell traction succeeds in overcoming the restoring mechanical force of the ECM and the force due to the attachment to the dish, and if there is a sufficiently high number of cells, then cells in higher density regions start pulling the cells in the lower density regions towards them, giving rise to an autocatalytic process. At the end there are areas without cells and areas with a high concentration of cells.

However, at very high densities one expects the uniform distribution of cells to be stable. From the modelling point of view this is obtained including saturation (e.g. $\alpha \neq 0$ in equation (20)). In fact, in this case, the instability region is the one above a curve with two asymptotes, the axis and the value of n_0 for which Σ_n has a maximum (see figure 12). In particular, if one has values of τ/E below the maximum, then no patterns form for any value of the density.

In fact, as discussed in Kowalczyk *et al.* [49], the exact form of the function $\Sigma_n(n)$ is not important in the stability analysis for a given cell density n_0. What matters is the value of its derivative at n_0, *i.e.* $d\Sigma_n/dn(n_0)$. In this respect, the choice of the function Σ_n strongly affects the stability curve in figure 12.

The models by Tranqui and Traqui [20] and Namy *et al.* [56] instead predict instability if

$$n_0 < \left(k - \frac{2k - 1}{2 + \frac{D}{h\rho_0}}\right)N,$$

and

$$\frac{\tau}{E} > \frac{1}{\rho_0 n_0}\frac{\frac{1-\nu}{(1+\nu)(1-2\nu)} + 2\sqrt{\frac{s}{\rho_0 E(1+\nu)}}\sqrt{\beta_1 + \frac{\nu}{1-2\nu}\beta_2}}{\frac{3}{2}N - n_0 + \frac{h\rho_0}{D}(N - 2n_0)}, \quad (38)$$

where $k = 3/2$ in Namy *et al.* [56] and $k = 1$ in Tranqui and Traqui [20].

The mechanisms triggering pattern formation in the models including haptotaxis is somewhat different. In particular haptotaxis has a destabilising effect.
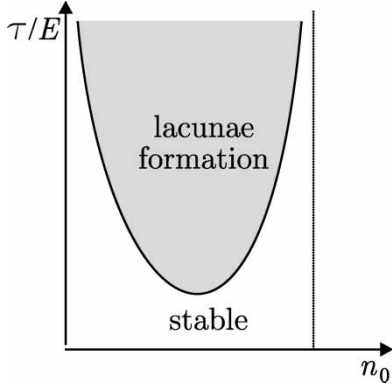
Figure 12. Neutral stability curve. The asyntote on the right is obtained when $\Sigma'(n_0) = 0$ for Manoussaki *et al.* [57], Murray *et al.* [58], Murray and Swanson [59], Murray [60], and Manoussaki [55] and for the values given in equation (39) for Tranqui and Traqui [20] and Namy et al. [56].

If haptotaxis is large enough compared to diffusion, the combination of cell motion and cell traction forces may start an autocatalytic process which is strong enough to overcome the viscoelastic resistance of the ECM.

On the other hand, both the restoring force and the material long-range parameters have a stabilizing effect. Looking at the dependence of the stability from the cell density, patterns form only in the area above a curve which has two asyntotes, in which one has graphs similar to figure 12 with the asyntotes in $n_0 = 0$ and

$$n_0 = \left(k - \frac{2k-1}{1 + \frac{D}{h\rho_0}} \right) N, \tag{39}$$

[20, 56].

From equation (39), it is clear that the stress-free value N (see equation (21)) strongly affects the threshold value for which lacunae appear.

In particular, for large enough cell density no pattern forms. Morphogenesis occurs for an intermediate range of cell densities and do not form again for very low densities. Unfortunately, in the experiments there is no transition to a stable distribution of cells for low densities (see figure 5).

In fact, as Tranqui and Traqui [20] themselves observe, "linear stability analysis is no longer valid out of a steady state neighbourhood" and for very small densities the uniform distribution cannot be achieved in experiments to start with.

Entering more in detail on the importance of the presence of the diffusion terms in the model, Manoussaki *et al.* [57] observed that "Anisotropy is not necessary for pattern to form" and Murray *et al.* [58] and Namy *et al.* [56] that the amplitude of the strain field within the ECM is too weak to influence qualitatively the tubulogenesis process, so that even diffusion is not fundamental. In fact, Murray [60] states that "One of the initially surprising and important findings is that random motility of cells was not necessary for the formation of patterns. Networks would still form

provided that the seeding density was sufficiently large." Also the effect of the viscoelastic characteristics of the ECM seem to play a minor role.

Thus, at least from the viewpoint of linear stability, but probably also from the viewpoint of numerical simulation, the minimal model describing traction-induced vasculogenesis might be

$$\frac{\partial n}{\partial t} + \nabla\cdot(n\mathbf{w}) = 0, \tag{40}$$

$$\tau\nabla\Sigma(n) - \frac{\mathbf{E}}{1+\nu}\nabla\cdot\left(\mathbf{E} + \frac{\nu}{1-2\nu}\mathrm{tr}(\mathbf{E})\mathbf{I}\right) = \mathbf{F}, \tag{41}$$

where the anchoring force can be either represented as an elastic restoring force or as a viscous drag. In the case of a drag force the dimensionless form of the equations above write

$$\frac{\partial \tilde{n}}{\partial \tilde{t}} + \nabla\cdot(\tilde{n}\tilde{w}) = 0 \tag{42}$$

$$\nabla\tilde{\Sigma}(\tilde{n}) - \nabla\cdot\left(\mathbf{E} + \frac{\nu}{1-2\nu}\mathrm{tr}(\mathbf{E})\mathbf{I}\right) = -\tilde{w} \tag{43}$$

with characteristic length and time scales

$$L = \frac{\tau n_0(1+\nu)}{E} \quad \text{and} \quad T = \frac{s\tau n_0(1+\nu)^2}{E^2\rho_0}. \tag{44}$$

In the case of an elastic drag force the minimal model rewrites

$$\frac{\partial \tilde{n}}{\partial \tilde{t}} + \nabla\cdot(\tilde{n}\tilde{w}) = 0 \tag{45}$$

$$\tilde{\tau}\nabla\tilde{\Sigma}(\tilde{n}) - \nabla\cdot\left(\mathbf{E} + \frac{\nu}{1-2\nu}\mathrm{tr}(\mathbf{E})\mathbf{I}\right) = -\tilde{s}\tilde{u} \tag{46}$$

where

$$\tilde{s} = \frac{s\tau n_0(1+\nu)^2}{E^2\rho_0}. \tag{47}$$

4.2 Simulations

From the simulations presented and discussed in the literature it appears that the formation of patterns for the mechanical models starts with the formation of regions with less cells surrounded by regions with more cells. The latter get thinner, while the former enlarge, forming lacunae. In some cases, the lacunae touch each other forming polygons with cells concentrated on the sides of the polygons. The evolution is always dynamical and the patterns do not reach a steady state, but continue growing Manoussaki [55]. Some lacunae grow larger and other close in a sphincter-like manner. Murray *et al.* [58] also observes that for very low stiffness or very high traction,

the pulling force of the cells is so strong that clusters form rather than knots linked by cords.

The main difference between the models using an elastic restoring force and those using a drag force modelling the anchorage of the ECM to the bottom of the Petri dish, is that in the former case one has the formation of polygon-like structures resembling the network formation at moderate densities of cells [57–60] and in the latter case one has the formation of holes resembling more closely the formation of lacunae [56].

Murray *et al.* [58], Murray [60], and Namy *et al.* [56] also give a simulation of the ramp experiment performed by Vernon *et al.* [36]. From the identification of the characteristic time of the minimal model, the following mechanism may be argued. Increasing the thickness (i.e. density) of the gel, decreases the characteristic time of the pattern formation (see equations (44) and (47)). So, in thicker regions the enlargements of the polygons occurs faster than in the thinner regions. This may explain the formation of larger polygons where the matrix is thicker. In addition, considering the stability condition, actually one could even have a transition to values of gel densities for which the uniform distribution is stable.

The paper by Manoussaki [55] mainly focuses on the numerical methods used for integrating the system of PDEs, which needs for instance to preserve mass, and on the result of the simulation. The first simulation (similarly to Manoussaki *et al.* [57] shows the formation of a vascular network for a density of cells of 100 cells/mm^2. The resulting patchwork size is close to 500 μm. A second simulation shows (always for 100 cells/mm^2) that if cell traction is too small, cell addense toward the centre with large lacunae forming near the boundary of the domain and no network formation. For higher values of cell traction a network forms in the central region of a typical size of 300 μm. The different size seems to be related with an increase in the shear and bulk viscosity, or with a different temporal snapshot of the simulation.

The parameter values measured in the experiments or estimated for the simulations are given in table 3. However, their strong variability points out the need of further measures to be performed on the experimental set-ups and of identifying standard materials and procedures. In fact, the simulations performed in the literature cannot help merging the data evaluated from different materials and experiments.

As already stated the papers by Holmes and Sleeman [61] and Manoussaki [55] extend the mechanical model considering the chemical interaction between cells and sources of angiogenic stimuli, so that their model is used to simulate the phenomenon of angiogenesis. For instance, simulations focusing on the effect of cell traction on externally induced angiogenesis show a narrowing of the capillary sprout.

5. Discussion

In our opinion, the two classes of models considered in sections 3 and 4 provide complementary description of *in vitro* vasculogenesis experiments. The PEC model successfully describes the early, migration dominated stages of network formation. Its basic assumption is that the mechanisms of persistence and endogenous chemotaxis govern the size of the capillary structure through the diffusion coefficient D and the chemoattractant half-life τ. The predicted average size of formed network structures is $\ell \approx \sqrt{D\tau}$, in good agreement with phenomenological observations *in vivo* and measurements *in vitro*.

Numerical simulations of the PEC model also reproduce the percolative transition occurring about

Table 3. Range of parameters relative to the elasto-mechanical model as experimentally measured or estimated (*) for the simulations.

Parameter	Range	Reference
E	10^3–10^4 Pa	Benkherourou *et al.* [63]
	0.8–2.7 Pa	Lee *et al.* [64]
ν	0.15–0.25	Scherer *et al.* [65] Shreiber *et al.* [66]
μ_1	10^5–10^8 Pa s 25 Pa s	Barocas *et al.* [67] Barocas and Tranquillo [68] Lee *et al.* [64]
μ_2	10^5–10^8 Pa s	(*) Murray *et al.* [58] (*) Holmes and Sleeman [61]
β_1, β_2	10^{-4}–10^{-3}/cm^2	(*) Tranqui and Traqui [20]
τ	0.15–0.27 dyne/cell 5×10^{-3} dyne/cell	Kolodney and Wysolmerski [69] (*) Murray *et al.* [58] (*) Manoussaki [55]
$\hat{\tau}$	10^{-9}–10^{-5} Pa cm^9/(g cell^2)	Ferrenq *et al.* [70]
	10^{-3} dyne cm^4/(mg cell) 0.015 dyne cm/cell	Tranquillo *et al.* [71] Shreiber *et al.* [66]
D	10^{-9}–10^{-6} cm^2/s	Di Milla *et al.* [72] Barocas *et al.* [67]
	2.6–19.3 $\times 10^{-9}$ cm^2/s	Hoying and Williams [73]
	$0.7 \cdot 10^{-12}$ cm^2/s	(*) Manoussaki [55]
K	10^{-8}–10^{-6} cm^5/(s g)	Dickinson and Tranquillo [74]
ρ_0	0.5–8 mg/cm^3	Delvoye *et al.* [75] Vernon *et al.* [36] Valihe *et al.* [35]
N	200–2000 cell/mm^3	Ferrenq *et al.* [70] Tranqui and Tracqui [20]
α	10^{-13}/cell^2	(*) Murray *et al.* [58]
	10^{-9}/cell^2	(*) Manoussaki [55]
s	10^{10} dyne s/cm^3	(*) Murray *et al.* [58]
	10^6–10^{11} dyne s/cm^3	(*) Manoussaki [55]

$n_c \approx 100\,\mathrm{cell/mm^2}$, which discriminate the situation in which a functional network is formed and another in which it is not properly connected. In general this type of model better describes the situation in which a moderate number of cells are seeded on the substratum.

The elasto-mechanical models describe the phenomenon of pattern formation starting from monolayer initial conditions. They describe the interaction with the substratum and a viscoelastic regime which is not accessible by the PEC model.

In our opinion, these phenomena become relevant also in experiments starting with few cells as soon as the early migration stage ends (ameboid motion), the cells adhere more on the substratum and an "embryonic" network structure is formed. On the biological side, migration and traction can be considered as different programmes that an individual cell is able to execute. One can argue that the start of either programme is dictated by the environment, e.g. by the fact that the cell is isolated or among a closely packed group of other cells. So, different initial conditions can put the system either in a "migrating" or in a "pulling" regime, thus explaining the different phenomenologies that inspired the two types of models.

From the contents of the section describing the experimental facts it is evident that there are experimental evidences that can be explained with the PEC model and not with the mechanical models and vice versa. In particular, phenomena which depend on the type of substratum cannot be described by PEC models and phenomena which depend on cell signaling cannot be described by mechanical models. Of course, some features can be explained by both models.

It can be argued that a complete, realistic description of the diverse phases of *in vitro* vasculogenesis should consist in suitably connecting the migration regime described by the PEC model and the successive viscoelastic regime described by the mechanical model or by some modification of it. This aim has been pursued by Tosin *et al.* [76].

Another issue that deserves attention is the formation of anisotropic structures in particular in the presence of more exogenous chemical factors. In fact, it is well known that in the human body, vascular networks have different characteristics according to the tissue to irrorate. In view of the applications to tissue mechanics it would be important to build capillary network with similar characteristics. In this respect, it would be interesting to test the PEC model by adding different chemical factors characterised by different physical properties and biological actions (e.g. attraction and repulsion) in order to govern the type of structures to be obtained as an outcome of the experiment [77].

With the same aim, if the thickness of the gel and its mechanical properties are found to be important, then one could govern the formation of the network by suitably grooving the lower surface of the dish having finer grids where the thickness is smaller and coarser grids where it is thicker.

Acknowledgements

References

[1] Risau, W. and Flamme, I., 1995, Vasculogenesis. *Annu. Rev. Cell Dev. Biol.*, **11**, 73–91.

[2] Poole, T.J., Finkelstein, E.B. and Cok, C.M., 2001, The role of FGF and VEGF in angioblast induction and migration during vasuclar development. *Dev Dyn.*, **220**, 1–17.

[3] Jain, R.K., 2003, Molecular regulation of vessel maturation. *Nature Med.*, **9**, 685–693.

[4] Krogh, A., 1919, The number and distribution of capillaries in muscle with calculations of the oxygen pressure head necessary for supplying the tissue. *J. Physiol.*, **52**, 409–415.

[5] Chilibeck, P.D., Paterson, D.H., Cunningham, D.A., Taylor, A.W. and Noble, E.G., 1997, Muscle capillarization O2 diffusion distance, and VO2 kinetics in old and young individuals. *J. Appl. Physiol.*, **82**, 63–69.

[6] Guyton, A. and Hall, J., 2000, *Textbook of Medical Physiology* (St. Louis: W.B. Saunders).

[7] Carmeliet, P., 2000, Mechanisms of angiogenesis and arteriogenesis. *Nature Med.*, **6**, 389–395.

[8] Ingber, D.E. and Folkman, J., 1989, How does extracellular matrix control capillary morphogenesis? *Cell*, **58**, 803–805.

[9] Kubota, Y., Kleinman, H., Martin, G. and Lawley, T., 1988, Role of laminin and basement membrane in the morphological differentiation of human endothelial cells into capillary-like structures. *J. Cell Biol.*, **107**, 1589–1598.

[10] Grant, D., Tashiro, K., Segui-Real, B., Yamada, Y., Martin, G. and Kleinman, H., 1989, Two different laminin domains mediate the differentiation of human endothelial cells into capillary-like structures *in vitro*. *Cell*, **58**, 933–943.

[11] Folkman, J. and Haudenschild, C., 1980, Angiogenesis *in vitro*. *Nature*, **288**, 551–556.

[12] Bussolino, F., Arese, M., Audero, E., Giraudo, S., Marchiò, S., Mitola, S., Primo, L. and Serini, G., 2003, Biological aspects of tumour angiogenesis. In: L. Preziosi (Ed.) *Cancer Modeling and Simulation* (Boca Raton: Chapman&Hall/CRC Press), pp. 1–22.

[13] Chaplain, M.A.J. and Anderson, A.R.A., 2003, Mathematical modelling of tissue invasion. In: L. Preziosi (Ed.) *Cancer Modeling and Simulation* (Boca Raton: Chapman&Hall/CRC Press), pp. 269–298.

[14] Little, C., Mironov, V. and Sage, H., 1998, *Vascular Morphogenesis: In Vivo, In Vitro and In Mente* (Boston: Birkhäuser).

[15] Levine, H. and Sleeman, B., 2004, Modelling tumour-induced angiogenesis. In: L. Preziosi (Ed.) *Cancer Modeling and Simulation* (Boca Raton: Chapman&Hall/CRC Press), pp. 147–184.

[16] Vailhé, B., Vittet, D. and Feige, J.J., 2001, *In vitro* models of vasculogenesis and angiogenesis. *Lab. Investig.*, **81**, 439–452.

[17] Hendrix, M.J.C., Seftor, E.A., Meltzer, P.S., Gardner, L.M.G., Hess, A.R., Kirschmann, D.A., Sachatteman, G.C. and Seftor, R.E.B., 2001, Expression and functional significance of Ve-cadherin in aggressive human melanoma cells: Role in vasculogenic mimicry. *Proc. Natl Acad. Sci.*, **98**, 8018–8024.

[18] Mariotis, A.J., Folberg, R., Hess, A., Seftor, E.A., Gardner, L.M.G., Pe'er, J., Trent, J.M., Meltzer, P.S. and Hendrix, M.J.C., 1999, Vascular channel formation by human melanoma cells *in vivo* and *in vitro*: vasculogenesis mimicry. *Am. J. Pathol.*, **155**, 739–752.

[19] Serini, G., Ambrosi, D., Giraudo, E., Gamba, A., Preziosi, L. and Bussolino, F., 2003, Modeling the early stages of vascular network assembly. *EMBO J.*, **22**, 1771–1779.

[20] Tranqui, L. and Traqui, P., 2000, Mechanical signalling and angiogenesis. The integration of cell-extracellular matrix couplings. *C.R. Acad. Sci. Paris, Science de la Vie*, **323**, 31–47.

[21] Friedl, P., 2004, Prespecification and plasticity: shifting mechanisms of cell migration. *Curr. Opin. Cell. Biol.*, **16**, 14–23.

[22] Webb, D.J. and Horwitz, A.F., 2003, New dimensions in cell migration. *Nature Cell Biol.*, **5**, 690–692.

[23] Wolf, K., Mazo, I., Leung, H., Engelke, K., von Andrian, U.H., deryugina, E.I., Strongin, A.Y., Bröcker, E.B. and Friedl, P., 2003, Compensation mechanism in tumor cell migration: mesenchimal-ameboid transition after blocking of pericellular proteolysis. *J. Cell. Biol.*, **160**, 267–277.

[24] Sambeth, R. and Bamgaertner, A., 2001, Autocatalytic polymerization generates persistent random walk of crawling cells. *Phys. Rev. Lett.*, **86**, 5196–5199.

[25] Helmlinger, G., Endo, M., Ferrara, N., Hlatky, L. and Jain, R., 2000, Formation of endothelial cell networks. *Nature*, **405**, 139–141.

[26] Ferrara, N., Gerber, H.P., et al., 2003, The biology of VEGF and its receptors. *Nature Med.*, **39**, 669–676.

[27] Roman, B.L. and Weinstein, B.M., 2000, Building the vertebrate vasculature: research is going swimmingly. *BioEssays*, 882–893.

[28] Neufeld, G., Cohen, T., Gengrinovitch, S. and Poltorak, Z., 1999, Vascular endothelial growth factor (VEGF) and its receptors. *FASEB J.*, **13**, 9–22.

[29] Gengrinovitch, S., Berman, B., David, G., Witte, L., Neufeld, G. and Ron, D., 1999, Glypican-1 is a VEGF165 binding proteoglycan that acts as an extracellular chaperone for VEGF165. *J. Biol. Chem.*, **274**, 10816–10822.

[30] Ambrosi, D., Gamba, A. and Serini, G., 2004, in press Cell directionality and chemotaxis in vascular morphogenesis. *Bull. Math. Biol.*, pp. 1851–1879.

[31] Gamba, A., Ambrosi, D., Coniglio, A., de Candia, A., Di Talia, S., Giraudo, E., Serini, G., Preziosi, L. and Bussolino, F., 2003, Percolation, morphogenesis and Burgers dynamics in blood vessels formation. *Phys. Rev. Lett.*, **90**, 118101.

[32] Ruhrberg, C., Gerhardt, H., Golding, M., Watson, R., Ioannidou, S., Fujisawa, H., Betsholtz, C. and Shima, D., 2002, Spatially restricted patterning cues provided by heparin-binding VEGF-A control blood vessel branching morphogenesis. *Gen. Devel.*, **16**, 2684–2698.

[33] Fong, G., Zhang, L., Bryce, D. and Peng, J., 1999, Increased hemangioblast commitment, not vascular disorganization, is the primary defect in *flt-1* knock-out mice. *Development*, **126**, 3015–3025.

[34] Stauffer, D. and Aharony, A., 1994, *Introduction to Percolation Theory* (London: Taylor&Francis).

[35] Vailhé, B., Lecomte, M., Wiernsperger, N. and Tranqui, L., 1998/1999, The formation of tubular structures by endothelial cells is under the control of fibrinolysis and mechanical factors. *Angiogenesis*, **2**, 331–344.

[36] Vernon, R., Angello, J., Iruela-Arispe, M.L., Lane, T. and Sage, E.H., 1992, Reorganization of basement membrane matrices by cellular traction promotes the formation of cellular networks *in vitro*. *Lab. Investig.*, **66**, 536–546.

[37] Vernon, R., Lara, S.L., Drake, C.J., Iruela-Arispe, M.L., Angello, J., Little, C.D. and Sage, E.H., 1995, Organized type 1 collagen influences of endothelial patterns during "spontaneous angiogenesis *in vitro*": Planar cultures as models of vascular development. *In Vitro Vascul. Dev. Biol.*, **31**, 120–131.

[38] Vernon, R. and Sage, E.-H., 1995, Between molecules and morphology extracellular matrix and creation of vascular form. *Am. J. Pathol.*, **1447**, 873–883.

[39] Othmer, H. and Stevens, A., 1997, Aggregation, blowup and collapse: The ABC's of generalized taxis. *SIAM J. Appl. Math.*, **57**, 1044–1081.

[40] Levine, H. and Sleeman, B., 1997, A system of reaction diffusion equations arising in the theory of reinforced random walks. *SIAM. J. Appl. Math.*, **57**, 683–730.

[41] Kowalczyk, R. (2004) "Preventing blow-up in a chemotaxis model" Preprint Politecnico di Torino.

[42] Filbet, F., Laurencot, P. and Pertham, B., 2004 "Derivation of hyperbolic models for chemosensitive movement", in press.

[43] Muller, Y., Christinger, H., Keyt, B. and de Vos, A., 1997, The crystal structure of vascular endothelial growth factor (VEGF) refined to 1.93 Å resolution: multiple copy flexibility and receptor binding. *Structure*, **5**, 1325.

[44] Walter, M., Cook, W., Ealick, S., Nagabhushan, T., Trotta, P. and Bugg, C., 1992, Three-dimensional structure of recombinant human granulocyte-macrophage colony-stimulating factor. *J. Mol. Biol.*, **224**, 1075.

[45] Pluen, A., Netti, P.A., Jain, R.K. and Berk, D.A., 1999, Diffusion of macromolecules in agarose gels: comparison of linear and globular configurations. *Biophys. J.*, **77**, 542–552.

[46] Cleaver, O. and Krieg, P., 1998, VEGF mediates angioblast migration during development of the dorsal aorta in Xenopus. *Development*, **125**, 3905–3914.

[47] Gazit, Y., Berk, D.A., Leunig, M., Baxter, L.T. and Jain, R.K., 1995, Scale-invariant behavior and vascular network formation in normal and tumor tissue. *Phys. Rev. E*, **75**, 2428–2431.

[48] Coniglio, A., de Candia, A., Di Talia, S. and Gamba, A., 2004, Percolation and Burgers' dynamics in a model of capillary formation. *Phys. Rev. E*, **69**, 051910.

[49] Kowalczyk, R., Gamba, A. and Preziosi, L., 2004, On the stability of homogeneous solutions to some aggregation models. *Discrete Contin. Dyn. Sys. B*, **4**, 203–220.

[50] Murray, J.D., Oster, G.F. and Harris, A.K., 1983, A mechanical model for mesenchymal morphogenesis. *J. Math. Biol.*, **17**, 125–129.

[51] Harris, A., Stopak, D. and Wild, P., 1981, Fibroblast traction as a mechanism for collagen morphogenesis. *Nature*, **290**, 249–251.

[52] Oster, G.F., Murray, J.D. and Harris, A.K., 1983, Mechanical aspects of mesenchymal morphogenesis. Cell traction models for generation of pattern and form in morphogenesis. *J. Embryol. Exp. Morphol.*, **78**, 83–125.

[53] Murray, J.D. and Oster, G.F., 1984a, Cell traction models for generation of pattern and form in morphogenesis. *J. Math. Biol.*, **19**, 265–279.

[54] Murray, J.D. and Oster, G.F., 1984b, Generation of biological pattern and form. *J. Math. Appl. Med. Biol.*, **1**, 51–75.

[55] Manoussaki, D., 2004, A mechanochemical model of vasculogenesis and angiogenesis. *Math. Model. Num. Anal.*, **37**, 581–599.

[56] Namy, P., Ohayon, J. and Traqui, P., 2004, Critical conditions for pattern formation and in vitro tubulogenesis driven by cellular traction fields. *J. Theor. Biol.*, **227**, 103–120.

[57] Manoussaki, D., Lubkin, S.R., Vernon, R.B. and Murray, J.D., 1996, A mechanical model for the formation of vascular networks *in vitro*. *Acta Biotheor.*, **44**, 271–282.

[58] Murray, J.D., Manoussaki, D., Lubkin, S.R. and Vernon, R.B., 1998, A mechanical theory of *in vitro* vascular network formation. In: C. Little, V. Mironov and H. Sage (Eds.) *Vascular Morphogenesis: In Vivo, In Vitro and In Mente* (Boston: Birkhäuser).

[59] Murray, J.D. and Swanson, K.R., 1999, On the mechanochemical theory of biological pattern formation with applications to wound healing and angiogenesis. In: M.A.J. Chaplain, G.D. Singh and J.C. McLachlan (Eds.) *On Growth and Form: Spatio-temporal Pattern Formation in Biology* (John Wiley&Sons).

[60] Murray, J.D., 2003, On the mechanical theory of biological pattern formation with application to vasculogenesis. *C.R. Biol.*, **326**, 2239–2252.

[61] Holmes, M. and Sleeman, B., 2000, A mathematical model of tumor angiogenesis incorporating cellular traction and viscoelastic effects. *J. Theor. Biol.*, **202**, 95–112.

[62] Levine, H., Sleeman, B. and Nilsen-Hamilton, M., 2001, Mathematical modeling of the onset of capillary formation initiating angiogenesis. *J. Math. Biol.*, **42**, 195–238.

[63] Benkherorou, M., Gumery, P.Y., Tranqui, L. and Tracqui, P., 2000, Quantification and macroscopic modeling of the nonlinear viscoelastic behavior of strained gels with varying fibrin concentrations. *IEEE Trans. Biomed. Eng.*, **47**, 1465–1475.

[64] Lee, B., Mitchell, L. and Buchsbaum, G., 1994, Rheology of the vitreous body. Part 2: Viscoelasticity of human vitreous. *Biorheology*, **29**, 521–533.

[65] Scherer, G., Hdach, H. and Phalippou, J., 1991, Thermal expansion of gels: A novel method for measuring permeability. *J. Non-Cryst. Solids*, **130**, 157–170.

[66] D.I. Shreiber, V.H. Barocas and R.T. Tranquillo, "Temporal variations in cell migration and traction during fibroblast-mediated gel compaction", *Biophys. J.*, **84**, 2003, pp. 4102–4114.

[67] Barocas, V.H., Moon, A.G. and Tranquillo, R.T., 1995, The fibroblast-populated collagen microsphere assay of cell traction force—Part 2: Measurement of the cell traction parameter. *J. Biomech. Eng.*, **117**, 161–170.

[68] Barocas, V.H. and Tranquillo, R.T., 1997, An anisotropic biphasic theory of tissue equivalent mechanics: The interplay among cell traction, fibrillar network deformation, fibril alignment, and cell contact guidance. *J. Biomech. Eng.*, **119**, 137–145.

[69] Kolodney M.S. and Wysolmerski R.B., "Isometric contraction by fibroblasts and endothelial cells in tissue culture: a quantitative study", *J. Cell Biol.*, **117**, 1992, pp. 73–82.

[70] Ferrenq, I., Tranqui, L., Vailhé, E., Gumery, P.Y. and Tracqui, P., 1997, Modelling biological gel contraction by cells: mechan-ocellular formulation and cell traction force quantification. *Acta Biotheor.*, **45**, 267–293.

[71] Tranquillo, R.T., Durrani, M.A. and Moon, A.G., 1992, Tissue engineering science: consequences of cell traction force. *Cytotech-nology*, **10**, 225–250.

[72] Di Milla, P.A., Quinn, J.A., Albelda, S.M. and Lauffenburger, D.A., 1992, Measurement of individual cell migration parameters for human tissue cells. *AIChE J.*, **38**, 1092–1104.

[73] Hoying, J.H. and Williams, S.K., 1996, Measurement of endothelial cell migration using an improved linear migration assay. *Microcirculation*, **3**, 167–174.

[74] Dickinson, R.B. and Tranquillo, R.T., 1993, A stochastic model for adhesion-mediated cell random motility and haptotaxis. *J. Math. Biol.*, **31**, 563–600.

[75] Delvoye, P., Wiliquet, P., Leveque, J.L., Nusgens, B.V. and Lapiere, C.M., 1991, Measurement of mechanical forces generated by skin fibroblasts embedded in a three-dimensional collagen gel. *J. Investig. Dermatol.*, **97**, 898–902.

[76] Tosin, A., Ambrosi, D. and Preziosi, L. (2004) "A mathematical model of vasculogenesis accounting for persistence, chemotaxis and substratum interactions", Preprint Politecnico di Torino.

[77] Lanza, V., Ambrosi, D. and Preziosi, L. (2004) "Anisotropic vasculogenesis", Preprint Politecnico di Torino.